Distribution of Cosmic-Ray Ionization Rates in the Galactic Diffuse Interstellar Medium as Inferred from Observations of H_3^+, OH^+, and H_2O^+

Nick Indriolo

Abstract Cosmic rays play a vital role in initiating the chemistry that occurs in molecular clouds. The ionization of H and H_2 begins a network of ion-molecule reactions responsible for generating many of the diatomic and small polyatomic molecules observed in the ISM. A few such species—OH^+, H_2O^+, and H_3^+ in particular—are formed and destroyed by rather simple processes, making them powerful probes of the cosmic-ray ionization rate. At present, we have performed observations searching for H_3^+ absorption in over 50 sight lines, and for OH^+ and H_2O^+ absorption in an additional 8 sight lines. Using these observations, we have inferred the distribution of cosmic-ray ionization rates in the diffuse ISM throughout the Galaxy. Some of the highest ionization rates are about 25 times larger than the lowest upper limits, suggesting variations in the underlying low-energy cosmic-ray flux across the Galaxy. We posit that such variations are caused by the distance between an observed cloud and the nearest site of particle acceleration, a conjecture supported by the high ionization rates found in close proximity to supernova remnants.

1 Introduction

In the diffuse, molecular interstellar medium (ISM), chemistry is driven by fast ion-molecule reactions [5, 15]. The reaction network begins with ionization of H and H_2 by cosmic rays, such that the ionization rates of these species (denoted ζ_H and ζ_2 for H and H_2, respectively) are important parameters for chemical modeling. There have been many estimates of the cosmic-ray ionization rate—both from observations of molecules (e.g., [4]) and from measurements of the local interstellar

N. Indriolo (✉)
Johns Hopkins University, Baltimore, MD 21218, USA
e-mail: indriolo@pha.jhu.edu

D.F. Torres and O. Reimer (eds.), *Cosmic Rays in Star-Forming Environments*, Astrophysics and Space Science Proceedings 34, DOI 10.1007/978-3-642-35410-6_7,

proton spectrum (e.g., [16])—with values ranging from a few times $10^{-18}\,s^{-1}$ up to a few times $10^{-14}\,s^{-1}$. Most recently, we used a survey of H_3^+ in 50 diffuse cloud sight lines to determine the distribution function of cosmic-ray ionization rates in the Galactic ISM [7]. In that study, we found a mean ionization rate of $\zeta_2 = 3.5\times10^{-16}\,s^{-1}$, with 68.3 % (Gaussian 1σ equivalent) of ionization rates in the range $0.5\times10^{-16}\,s^{-1} < \zeta_2 < 8.8\times10^{-16}\,s^{-1}$. Herein we review the primary results from Indriolo and McCall [7], as well as the methods used in obtaining those results, and update our analysis to include recent estimates of the cosmic-ray ionization rate of atomic hydrogen from observations of OH^+ and H_2O^+.

1.1 Hydrogen Chemistry

In the ISM the formation of H_3^+ begins with the ionization of H_2 by cosmic rays

$$H_2 + CR \rightarrow H_2^+ + e^- + CR', \tag{1}$$

a process quickly followed by a reaction of H_2^+ with H_2,

$$H_2^+ + H_2 \rightarrow H_3^+ + H. \tag{2}$$

Reaction (2) is many orders of magnitude faster than reaction (1), such that cosmic-ray ionization of H_2 is the rate-limiting step, and can be taken as the formation rate of H_3^+. In diffuse molecular clouds H_3^+ is predominantly destroyed by dissociative recombination with electrons

$$H_3^+ + e^- \rightarrow H_2 + H \text{ or } H + H + H, \tag{3}$$

and although proton transfer to O and CO do occur, they have a negligible effect on the destruction rate of H_3^+ in such environments (see Fig. 14 of [7]).

1.2 Oxygen Chemistry

The formation of oxygen bearing ions in the diffuse ISM begins with the ionization of atomic hydrogen by cosmic rays

$$H + CR \rightarrow H^+ + e^- + CR'. \tag{4}$$

This is followed by the endothermic charge transfer to oxygen to form O^+,

$$H^+ + O \rightarrow O^+ + H, \tag{5}$$

and hydrogen abstraction from H_2,

$$O^+ + H_2 \rightarrow OH^+ + H. \tag{6}$$

OH^+ is either destroyed by further hydrogen abstraction to form H_2O^+,

$$OH^+ + H_2 \rightarrow H_2O^+ + H, \tag{7}$$

or by dissociative recombination with electrons.

$$OH^+ + e^- \rightarrow \text{products}. \tag{8}$$

The same is true for H_2O^+,

$$H_2O^+ + H_2 \rightarrow H_3O^+ + H, \tag{9}$$

$$H_2O^+ + e^- \rightarrow \text{products}, \tag{10}$$

but H_3O^+ is only destroyed by dissociative recombination with electrons.

$$H_3O^+ + e^- \rightarrow \text{products}. \tag{11}$$

1.3 Steady-State Relations

In order to relate the abundances of various species, we assume that chemistry is in steady-state (i.e., the formation rate of each species is equal to its destruction rate). Given the short expected lifetimes of the ions under consideration, about 100–1,000 years, with respect to the estimated lifetime of diffuse clouds, $\sim 10^6$ years, the steady-state approximation is reasonable. Taking reactions (1) and (3) to govern the H_3^+ abundance, steady state is given by

$$\zeta_2 n(H_2) = k(H_3^+|e^-) n(H_3^+) n(e), \tag{12}$$

where $n(X)$ is the number density of species X, and $k(X|Y)$ is the rate coefficient for the reaction between species X and Y. Making substitutions as in Indriolo and McCall [7] we arrive at

$$\zeta_2 = k(H_3^+|e^-) x_e n_H \frac{N(H_3^+)}{N(H_2)}, \tag{13}$$

where $N(X)$ is the column density of species X, $n_H \equiv n(H) + 2n(H_2)$ is the number density of hydrogen nuclei, and $x_e \equiv n(e)/n_H$ is the fractional abundance of

electrons with respect to hydrogen. Equation (13) is used in determining the cosmic-ray ionization rate of H_2 from observations of H_3^+.

Assuming the H_2O^+ abundance is controlled by reactions (7), (9), and (10) results in the OH^+/H_2O^+ abundance ratio relation given in Gerin et al. [2], which can be re-arranged to produce

$$f_{H_2} = \frac{2x_e k(H_2O^+|e^-)/k(OH^+|H_2)}{N(OH^+)/N(H_2O^+) - k(H_{2O}{}^+|H_2)/k(OH^+|H_2)}, \tag{14}$$

where $f_{H_2} \equiv 2n(H_2)/n_H$ is the molecular hydrogen fraction.

Taking reactions (4), (7), and (8) to control the OH^+ abundance, steady state is given by

$$\epsilon\zeta_H n(H) = n(OH^+)[n(H_2)k(OH^+|H_2) + n(e)k(OH^+|e^-)]. \tag{15}$$

Here, the destruction of OH^+ is thought to be complete, but not all H^+ will eventually lead to OH^+. To account for processes competing with reactions (5) and (6)—i.e., that prevent H^+ from forming OH^+—we introduce an efficiency factor, ϵ, to the left hand side of Eq. (15), as in Neufeld et al. [11]. This parameter gives the fraction of H^+ formed by cosmic-ray ionization of H that produces OH^+. Solving for the product $\epsilon\zeta_H$ and making substitutions results in

$$\epsilon\zeta_H = \frac{N(OH^+)}{N(H)} n_H \left[\frac{f_{H_2}}{2} k(OH^+|H_2) + x_e k(OH^+|e^-)\right], \tag{16}$$

which allows us to find ζ_H after making assumptions about ϵ.

In Eqs. (13), (14), and (16), we adopt the rate coefficients used by the 2006 version of the UMIST Database for Astrochemistry ([17], database available online at: www.udfa.net). $N(H)$ is determined from 21 cm observations of H I, and $N(H_2)$ from direct observations of H_2 in the UV, or from observations of CH and the empirical relation $N(CH)/N(H_2) = 3.5^{+2.1}_{-1.4} \times 10^{-8}$ found by Sheffer et al. [13]. The electron fraction, x_e, is either determined from observations of C^+ or set equal to the average value of $x(C^+) = 1.5 \times 10^{-4}$ [14], assuming nearly all electrons are the result of singly photoionized carbon. The hydrogen number density, n_H, is difficult to determine, and unless an estimate is available in the literature for a particular sight line, we adopt a rough average value of 200 cm^{-3} for the molecular interior of a diffuse cloud. Assuming pressure balance, this translates to $n_H \sim 70\,cm^{-3}$ in the warmer, primarily atomic outskirts of such a cloud (H_3^+ is thought to reside in the molecular interior of clouds, while OH^+ and H_2O^+ are in the atomic outer layers). Recent modeling efforts [6] and observations [9] suggest a low value for the efficiency factor, and herein we adopt $\epsilon \sim 0.1$. To directly compare ζ_2 and ζ_H, we convert values determined from H_3^+ and from OH^+ and H_2O^+ to the primary

cosmic-ray ionization rate, ζ_p. This is the ionization rate of atomic hydrogen due to cosmic rays alone (i.e., not accounting for ionization by secondary electrons), and is related to the total ionization rates of H and H_2 by $\zeta_H = 1.5\zeta_p$ and $\zeta_2 = 2.3\zeta_p$, respectively [3].

2 Summary of Observations

We have performed observations searching for H_3^+, OH^+, and H_2O^+ in absorption in order to determine the column densities of these species and calculate ionization rates from Eqs. (13), (14), and (16). Observations of H_3^+ targeted ro-vibrational transitions near 3.7 μm in 50 diffuse cloud sight lines, and were made using a variety of ground based telescopes with high resolution IR spectrographs (e.g., CRIRES at VLT). A list of the targeted sight lines along with H_3^+ column densities and inferred cosmic-ray ionization rates (or upper limits on these parameters) is presented in Indriolo and McCall [7]. Observations searching for OH^+ and H_2O^+ absorption were made using HIFI aboard *Herschel* as part of the PRISMAS (PRobing InterStellar Molecules with Absorption line Studies) key programme, and targeted rotational transitions near 971 and 1,115 GHz, respectively. The PRISMAS programme observed eight sight lines in total, and preliminary results for the oxygen chemistry in two of those, W 31C and W 49N, have been reported in Gerin et al. [2] and Neufeld et al. [11].

3 Distribution of Ionization Rates

In Indriolo and McCall [7] we reported the distribution of cosmic-ray ionization rates in the diffuse ISM as determined from observations of H_3^+ (see Fig. 16 therein). With observations of OH^+ and H_2O^+ toward the eight PRISMAS sight lines, we have now also determined the ionization rate in several clouds where the necessary supplementary data such as $N(H)$ are available. The full analysis of these data (i.e., $N(OH^+)$, $N(H_2O^+)$, ζ_H, etc.) will be presented in a future manuscript. For the time being, we have simply combined the ionization rates inferred from OH^+ and H_2O^+ with those reported in Indriolo and McCall [7] to update the overall distribution of cosmic-ray ionization rates. The results are shown in Fig. 1, where the solid black curve is $\zeta_p f(\zeta_p)$, i.e., the probability density function of ionization rates scaled by the ionization rate. See the Fig. 1 caption for a complete description of what is shown.

In Fig. 1 we see that the addition of 9 ionization rates to the previous sample of 52[1] does not significantly alter the distribution of ionization rates. Both the peak

[1]Two of the fifty sight lines observed have two distinguishable velocity components in H_3^+

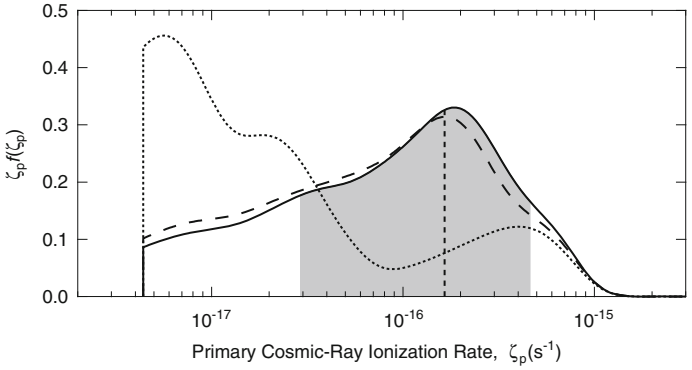

Fig. 1 Shown here is $\zeta_p f(\zeta_p)$—the product of the probability density function of cosmic-ray ionization rates, $f(\zeta_p)$, and the ionization rate, ζ_p—as a function of the ionization rate. The definition of $f(\zeta_p)$ is such that the probability of the cosmic-ray ionization rate being in any particular range is given by $P(a \leq \zeta_p \leq b) = \int_a^b f(\zeta_p) d\zeta_p$. Scaling $f(\zeta_p)$ by ζ_p makes it easy to see "by eye" what portion of $f(\zeta_p)$ carries the largest probability given the logarithmic x-axis. The solid curve combines ionization rates and upper limits from the 50 sight lines observed in H_3^+ by Indriolo and McCall [7] with preliminary ionization rates inferred for 9 cloud components observed in OH^+ and H_2O^+ as part of the PRISMAS key programme. The mean value of $\zeta_p = 1.65 \times 10^{-16}\,s^{-1}$ is marked by the vertical dotted line, and the shaded region that extends from 0.29×10^{-16} to $4.6 \times 10^{-16}\,s^{-1}$ shows the minimum range of ionization rates (in log space) that contains 68.3 % (Gaussian 1σ equivalent) of the area under $f(\zeta_p)$. The dashed curve is found using only the ionization rates inferred from H_3^+ in Indriolo and McCall [7], and is identical to the distribution in that paper, except in terms of ζ_p instead of ζ_2. The dotted curve is for four sight lines (o Sco, HD 147889, ρ Oph D, and χ Oph) in the Ophiuchus-Scorpius region where H_3^+ is not detected, and some of the lowest upper limits on the cosmic-ray ionization rate are found. The sharp cutoff on the low end of the distribution is a "floor" value ($\zeta_p = (1.0/2.3) \times 10^{-17}\,s^{-1}$), above which the ionization rate in diffuse clouds is expected to remain due to the continuous diffusion of energetic particles throughout the Galactic disk

of $\zeta_p f(\zeta_p)$ and the mean ionization rate shift to slightly higher values as most of the ionization rates inferred from OH^+ and H_2O^+ are relatively close to $\zeta_p \sim 2 \times 10^{-16}\,s^{-1}$. It is surprising that the adopted value of $\epsilon = 0.1$ results in ionization rates so consistent with the mean value found in Indriolo and McCall [7], but because of the uncertainty in ϵ these results must be viewed as highly preliminary.

Also of interest is the vastly different shape of $\zeta_p f(\zeta_p)$ as determined from four sight lines in the Ophiuchus-Scorpius region. H_3^+ has not been detected in any of these sight lines, and 3σ upper limits on the ionization rates toward o Sco and HD 147889 are $\zeta_p < 1.44 \times 10^{-17}\,s^{-1}$ and $\zeta_p < 4.70 \times 10^{-17}\,s^{-1}$, respectively—some of the lowest values in our entire sample. In fact, the largest value inferred for ζ_p—toward HD 183143—is more than 30 times larger than the upper limit toward o Sco. This suggests that the ionization rate varies significantly between sight lines, and that the distribution of ionization rates may vary between specific regions of the sky.

4 Discussion

The wide distribution of ionization rates shown in Fig. 1 and the potential variation between different regions of the Galaxy require some underlying physical explanation. We posit that such variations are caused by the distance between an observed cloud and the nearest site of particle acceleration for the following reasons. The cross section for ionization of H and H_2 by cosmic rays increases as the particle energy decreases, such that particles with energies of a few MeV are the most efficient at ionization (see, e.g., [12]). This also means that low-energy particles lose their energy to ionization faster than high energy particles and cannot travel very far from their acceleration sites. For example, a 20 MeV proton can traverse a column of about $6 \times 10^{22}\,\mathrm{cm}^{-2}$, over 60 times more material than a 2 MeV proton, which can traverse a column of about $9 \times 10^{20}\,\mathrm{cm}^{-2}$ [1]. Particles with even higher energies ($E > 1\,\mathrm{GeV}$) are thought to diffuse throughout the Galactic disk, creating a relatively uniform underlying cosmic-ray spectrum that sets the floor value assumed above [16]. Given this picture, the cosmic-ray ionization rate at any arbitrary position in the Galaxy is determined by the sum of the underlying interstellar particle spectrum and contributions to the particle flux from any nearby sites of particle acceleration.

In the above scenario, molecular material in close proximity to a supernova remnant—likely candidates for particle acceleration—should show higher ionization rates than in the average diffuse ISM. To test this theory, we made observations searching for H_3^+ in six sight lines near the supernova remnant IC 443 [8]. H_3^+ was detected in two sight lines—ALS 8828 and HD 254577—and inferred ionization rates were $\zeta_p = 7.0^{+3.5}_{-5.2} \times 10^{-16}\,\mathrm{s}^{-1}$ and $\zeta_p = 11^{+5.7}_{-8.3} \times 10^{-16}\,\mathrm{s}^{-1}$, the two largest values found in the Galactic disk from H_3^+ observations to date. Upper limits inferred for the other four sight lines are consistent with ionization rates found in the diffuse ISM. Recent observations of IC 443 in ^{12}CO $J = 1-0$ suggest that only the two sight lines with H_3^+ detections probe gas that is interacting with the supernova remnant, while the other four likely probe foreground material [10]. As such, these results confirm the picture where the cosmic-ray ionization rate is controlled by proximity to a site of particle acceleration.

5 Summary

We have combined cosmic-ray ionization rates inferred from a preliminary analysis of 9 cloud components observed in OH^+ and H_2O^+ with those inferred in 50 sight lines from observations of H_3^+ reported in Indriolo and McCall [7]. The result is an updated distribution function for the primary cosmic-ray ionization rate that has a mean value of $\zeta_p = 1.65 \times 10^{-16}\,\mathrm{s}^{-1}$ and a 1σ range of $0.29 \times 10^{-16}\,\mathrm{s}^{-1} < \zeta_p < 4.6 \times 10^{-16}\,\mathrm{s}^{-1}$. The wide range of ionization rates is indicative of variations in the flux of low-energy cosmic-rays, something likely controlled by the distance between

an observed cloud and the nearest site of particle acceleration. Observations of H_3^+ in molecular material that is interacting with the supernova remnant IC 443 give the highest ionization rates found in the Galactic disk to date, thus supporting this scenario.

Acknowledgements I would like to thank David Neufeld for performing a significant portion of the OH^+ and H_2O^+ data processing, Maryvonne Gerin for encouraging my involvement in the PRISMAS key programme for Herschel, and Ben McCall for support during graduate school when the bulk of the H_3^+ analysis was done.

References

1. Cravens, T. E., & Dalgarno, A. 1978, ApJ, 219, 750
2. Gerin, M., de Luca, M., Black, J., et al. 2010, A&A, 518, L110
3. Glassgold, A. E., & Langer, W. D. 1974, ApJ, 193, 73
4. Hartquist, T. W., Doyle, H. T., & Dalgarno, A. 1978, A&A, 68, 65
5. Herbst, E. & Klemperer, W. 1973, ApJ, 185, 505
6. Hollenbach, D., Kaufman, M. J., Neufeld, D. A., Wolfire, M., & Goicoechea, J. R. 2012, ApJ, 754, 105
7. Indriolo, N., & McCall, B. J. 2012, ApJ, 745, 91
8. Indriolo, N., Blake, G. A., Goto, M., et al. 2010, ApJ, 724, 1357
9. Indriolo, N., Neufeld, D. A., Gerin, M., et al. 2012, ApJ, 758, 83
10. Lee, J.-J., Koo, B.-C., Snell, R. L., et al. 2012, ApJ, 749, 34 (arXiv:1202.4789v1)
11. Neufeld, D. A., Goicoechea, J. R., Sonnentrucker, P., et al. 2010, A&A, 521, L10
12. Padovani, M., Galli, D., & Glassgold, A. E. 2009, A&A, 501, 619
13. Sheffer, Y., Rogers, M., Federman, S. R., et al. 2008, ApJ, 687, 1075
14. Sofia, U. J., Lauroesch, J. T., Meyer, D. M., & Cartledge, S. I. B. 2004, ApJ, 605, 272
15. Watson, W. D. 1973, ApJ, 183, L17
16. Webber, W. R. 1998, ApJ, 506, 329
17. Woodall, J., Agúndez, M., Markwick-Kemper, A. J., & Millar, T. J. 2007, A&A, 466, 1197